A. Supplementary material

We provide additional material to supplement our main submission. In particular, the following aspects are covered:

- DeepLPF parameter prediction block architecture (Section A.1)
- DeepLPF multiple filter fusion architecture (Section A.2)
- Visualisation of learnable inversion for the graduated filter (Section A.3)
- Additional qualitative visual results (Section A.4)

A.1. DeepLPF parameter prediction block architecture

Figure 8 presents the architecture of the DeepLPF parameter prediction network. The network accepts from the backbone feature extraction neural network (*e.g.* a U-Net [21]) a feature map of dimension $H \times W \times C$, where H is the height, W is the width and C is the channel count. The extracted features are passed through an alternating series of convolution and maxpooling blocks, followed by a global average pooling and fully connected layer. Leaky ReLUs serve as the activation functions and dropout is employed before the fully connected layer (applied 50% at both training and test time). We show in Figure 11 the U-Net backbone feature extraction network we use for experiments on the MIT-Adobe-5K-DPE dataset.

A.2. DeepLPF multiple filter fusion architecture

Figure 9 presents the filter fusion architecture, which receives the scaling maps of multiple filters of the same type (here we show elliptical filters but the same architecture is used for graduated filters) and combines the filters through multiplication into a single scaling map to be applied to the input image to yield the enhanced image.

A.3. Visualisation of learnable inversion for the graduated filter

Table 5 presents results for the graduated filter with and without learnable inversion. Inversion determines where the 100% scaling factor area of the filter is located with respect to the central line of the graduated filter. We find in Table 5 that PSNR and SSIM both benefit by permitting this additional filter flexibility.

Figure 10 shows two heatmaps illustrating the effect of learnable inversion on shifting the location of the 100% scaling area of the graduated filter with respect to the central line.

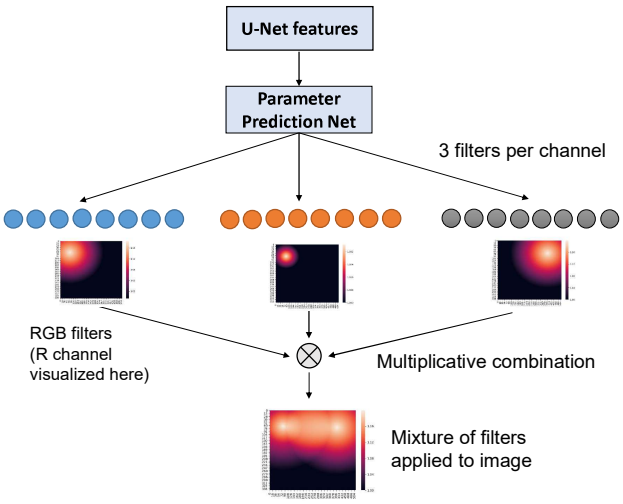

Figure 9: Fusion architecture for several instances of the elliptical filter.

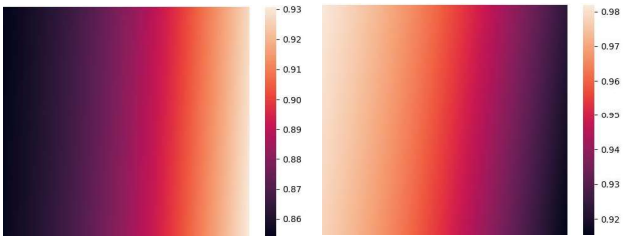

(a) (b)

Figure 10: Learnable inversion for the graduated filter. The learnable binary indicator variable $\hat{g}_{inv}$ determines the position of the 100% scaling area of the graduated filter relative to the central line. In heatmap (a) the 100% area is towards the left whereas in (b) the 100% area is towards the right.

Table 5: Image quality can be further improved by enabling inversion of the graduated filter. See Section 3.2.2

Architecture	PSNR↑	SSIM↑
Graduated filter (no inversion)	22.52	0.878
Graduated filter (inversion)	**22.64**	**0.888**

A.4. Additional visual examples

Further filter visualizations, output image examples from DeepLPF and the baseline models on the SID, MIT-Adobe-5K-DPE and MIT-Adobe-5K-UPE datasets are presented in Figures 12-20:

- Figure 12: Comparison between DeepLPF and DeepUPE [25] on sample images from the MIT-Adobe-5K-UPE dataset.

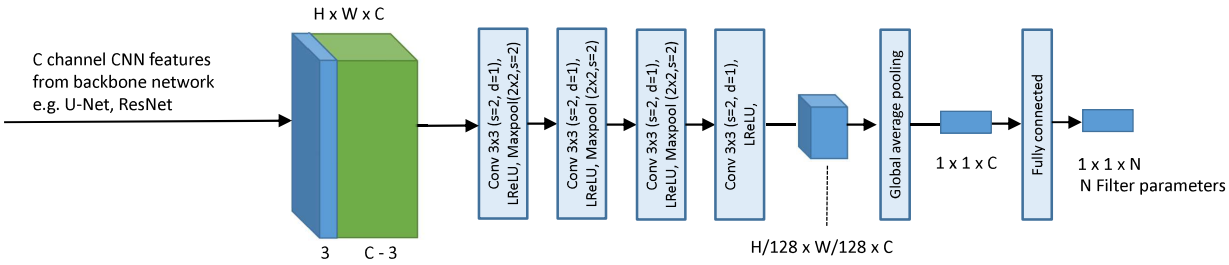

Figure 8: Filter Parameter regression architecture of DeepLPF. Given features from a backbone network (*e.g.* Figure 11), the parameter regression network infers the parameters of the parametric filters (polynomial, elliptical, or graduated).

- Figure 13: Additional qualitative comparison between DeepLPF and DPE [8] on sample images of the MIT-Adobe-5K-DPE dataset.
- Figure 14: Additional qualitative comparison between U-Net [21] and DeepLPF on sample images from the MIT-Adobe-5K-DPE dataset.
- Figure 15: Additional visual results from the MIT-Adobe-5K-DPE dataset comparing DeepLPF to DPE[8], CLHE[35], DPED (iphone7)[13], NPEA[33], FLLF[34]
- Figure 16: Additional visual results from the MIT-Adobe-5K-DPE dataset comparing DeepLPF to DPE[8], CLHE[35], DPED (iphone7)[13], NPEA[33], FLLF[34]
- Figure 17: Qualitative comparison between DeepLPF and SID [4] architecture on sample images of the Fuji partition of the SID dataset.
- Figure 18: Ablation study showing the effect of different combinations of parametric filter compared to the groundtruth and the baseline U-Net [21] on the MIT-Adobe-5K-DPE dataset.
- Figure 19: Additional examples of elliptical filters acting on different channels of the input images.
- Figure 20: Additional examples of mixtures of graduated or elliptical filters acting on different channels of the input images.
- Figure 21: Additional examples of polynomial (cubic-10) filters acting on different channels of the input images.
- Figure 22: Examples of DeepLPF failure cases.

References

[33] Y. Gao, H. Hu, and B. Li, and Q. Guo. Naturalness Preserved Non-Uniform Illumination Estimation for Image Enhancement Based on Retinex. *IEEE Transactions on Multimedia*, 2017. 12, 17, 18

[34] M. Aubry, S. Paris, S. Hasinoff, J. Kautz, and F. Durand. Fast Local Laplacian Filters: Theory and Applications. *ACM Trans. Graph.*, 2014. 2, 12, 17, 18

[35] S. Wang, W. Cho, J. Jang, M. Abidi, and J. Paik. Contrast-dependent saturation adjustment for outdoor image enhancement. *Journal of the Optical Society of America A*, 2017. 12, 17, 18

[36] M. Liu, T. Breuel, and J. Kautz. Unsupervised image-to-image translation networks. *Advances in neural information processing systems*, 2017.

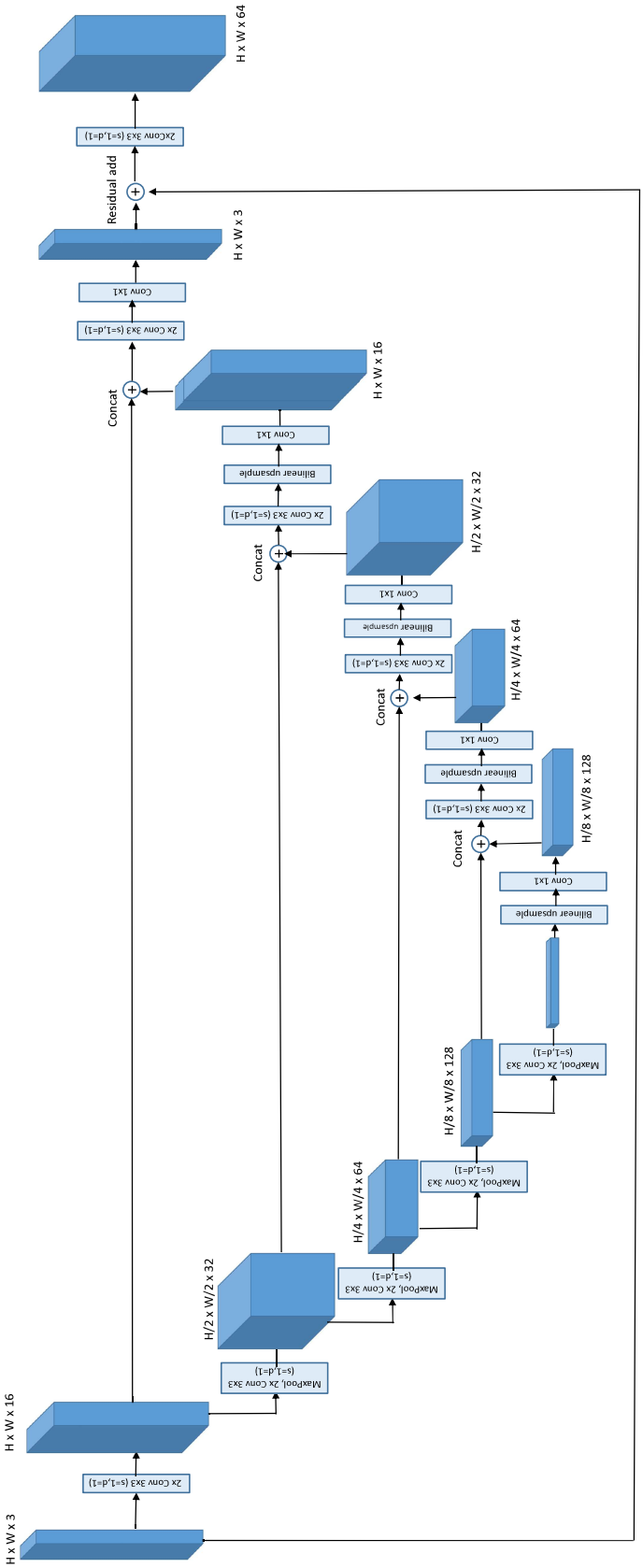

Figure 11: U-Net backbone feature extraction network used for the MIT-Adobe-5K-DPE dataset. The RGB image data is input on the left and the features for input to the DeepLPF block are output on the right.

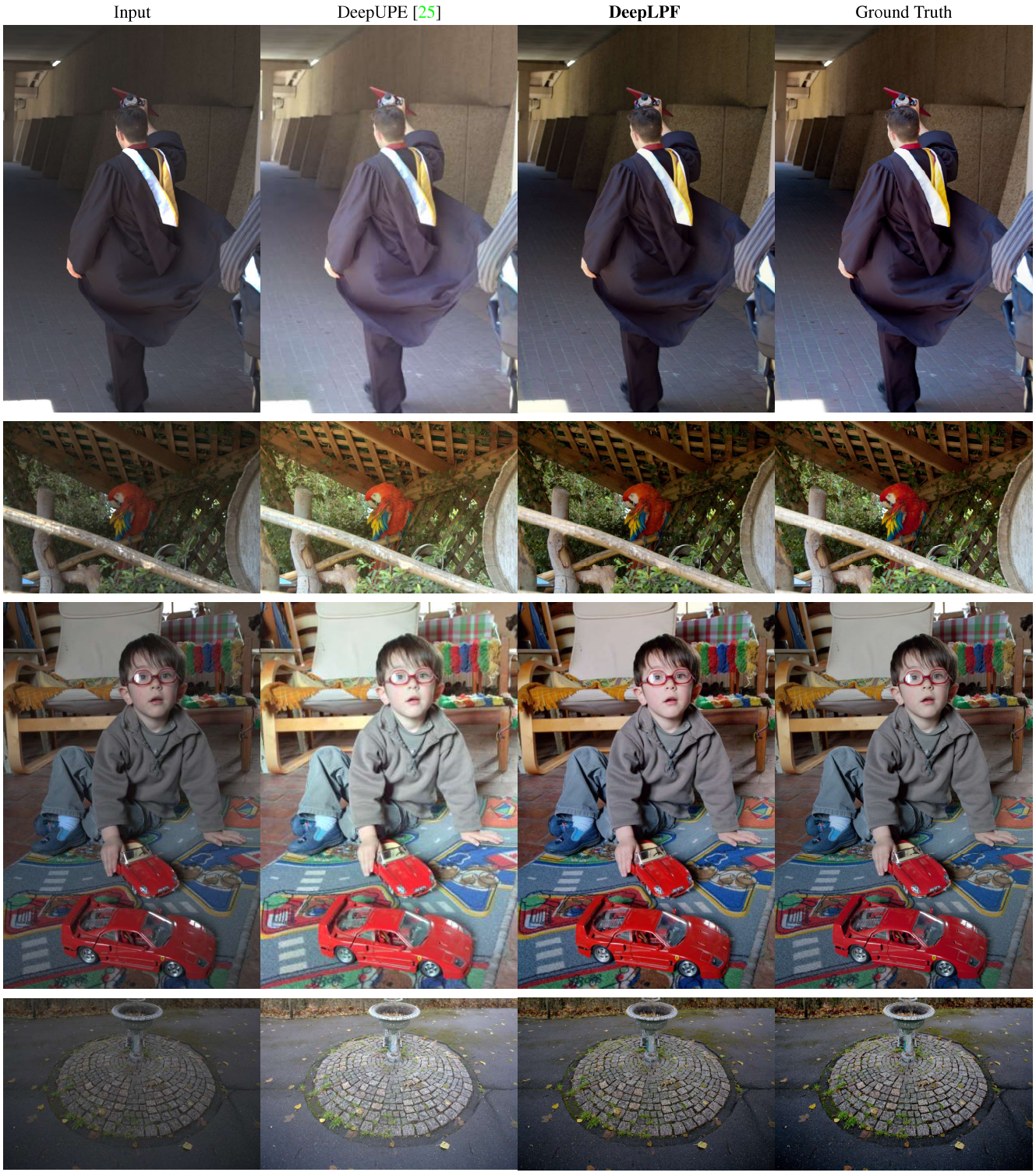

Figure 12: Additional qualitative comparison between **DeepLPF** and **DeepUPE** on sample images from the **MIT-Adobe-5K-UPE** dataset.

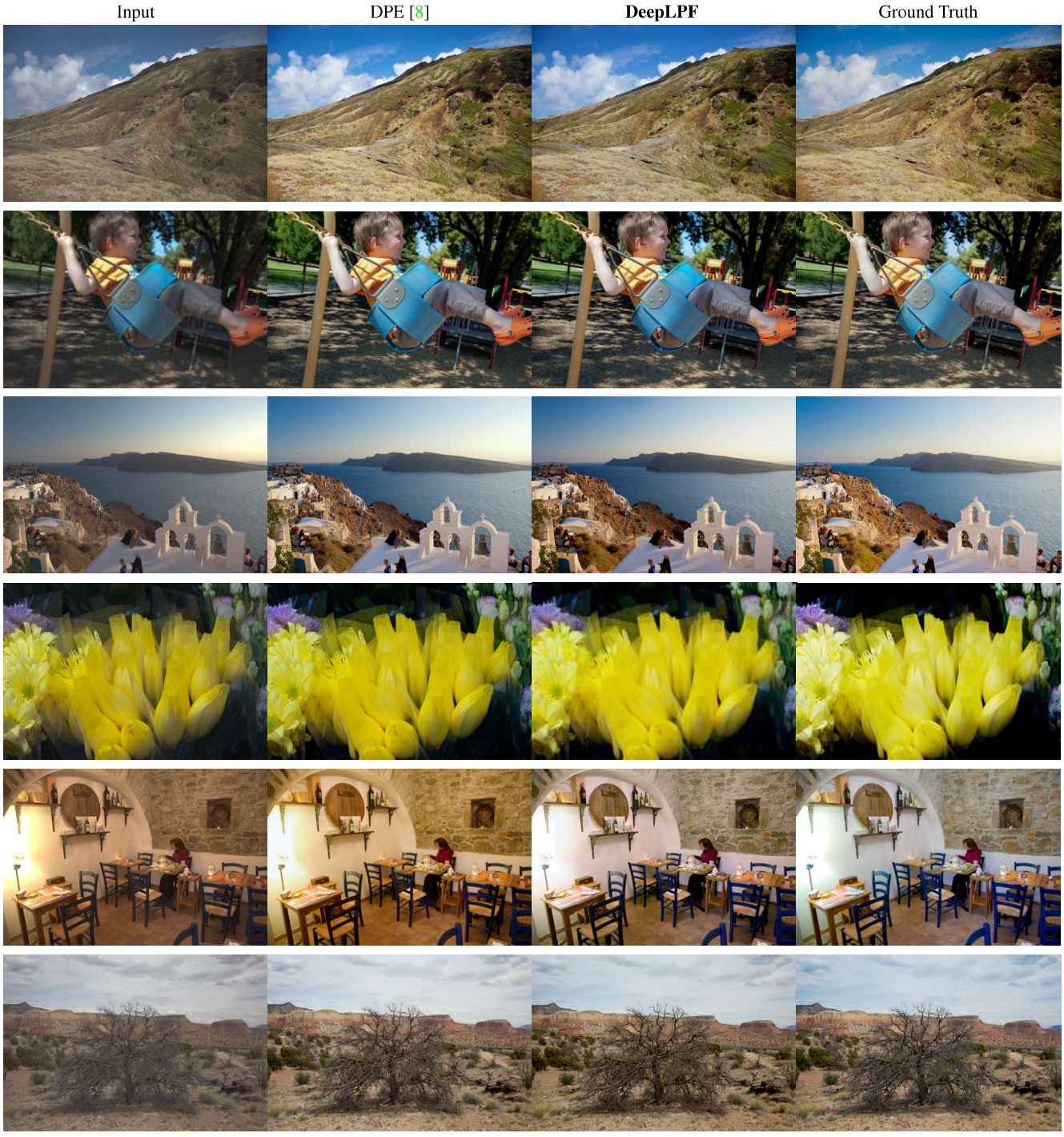

Figure 13: Additional qualitative comparison between **DeepLPF** and **DPE** [8] on sample images of the **MIT-Adobe-5K-DPE** dataset.

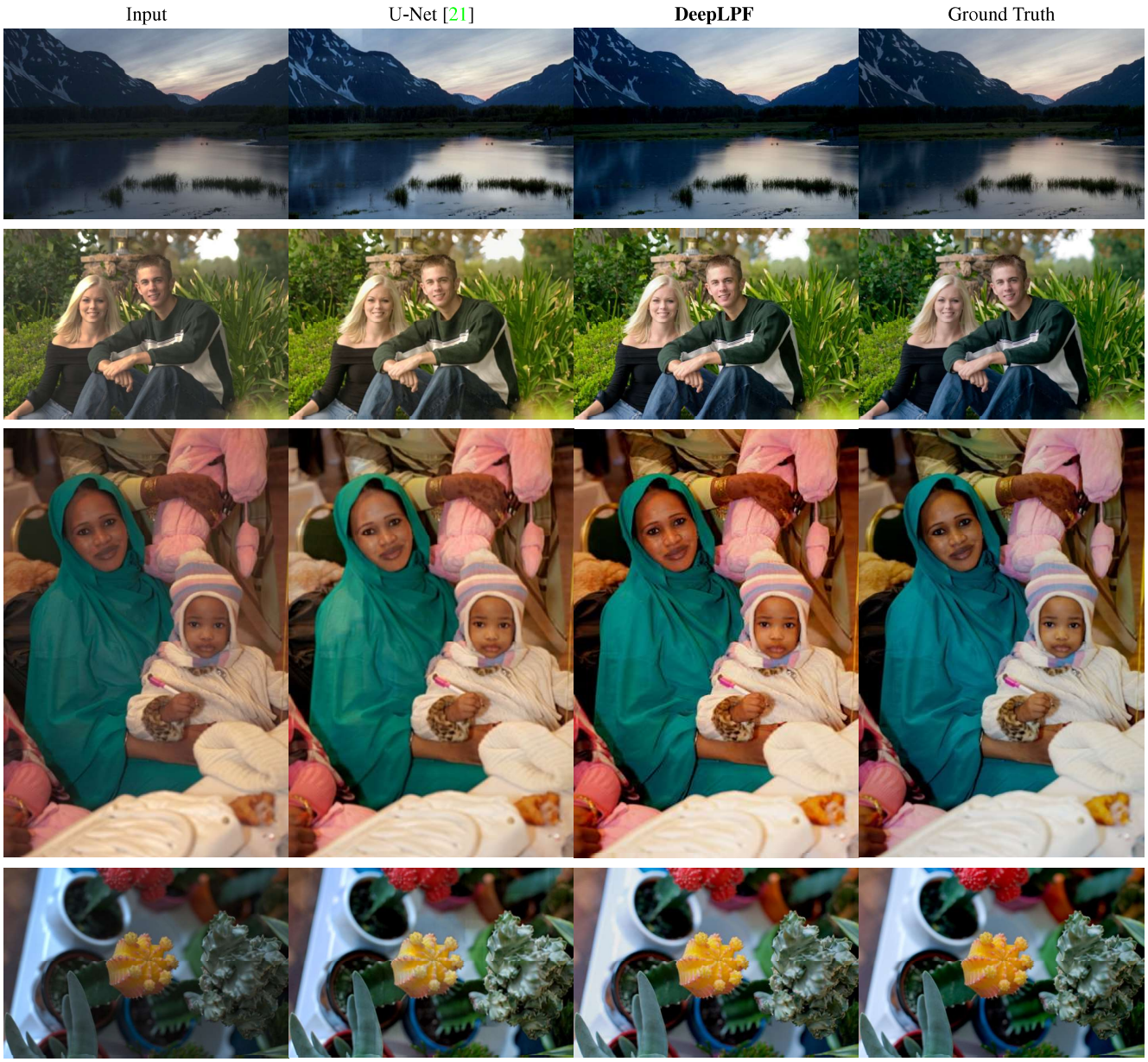

Figure 14: Additional qualitative comparison between **U-Net** [21] and **DeepLPF** on sample images from the **MIT-Adobe-5K-DPE** dataset.

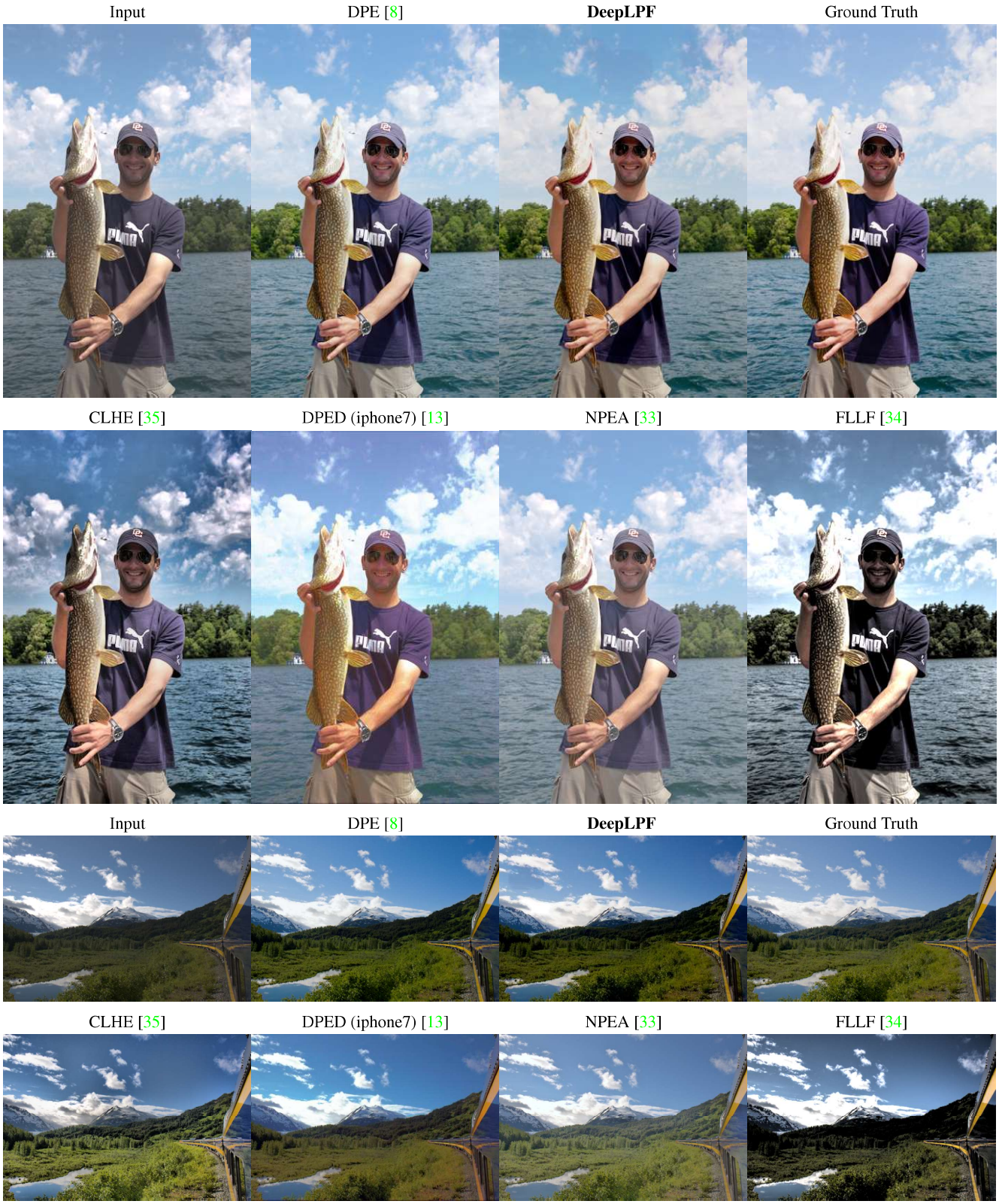

Figure 15: Additional visual results from the **MIT-Adobe-5K-DPE** dataset comparing **DeepLPF** to **DPE** [8], **CLHE** [35], **DPED (iphone7)** [13], **NPEA** [33], **FLLF** [34]

Figure 16: Additional visual results from the **MIT-Adobe-5K-DPE** dataset comparing **DeepLPF** to **DPE** [8], **CLHE** [35], **DPED (iphone7)** [13], **NPEA** [33], **FLLF** [34]

Figure 17: Qualitative comparison between **DeepLPF** and **SID** [4] on sample images of the Fuji partition of the **SID** dataset.

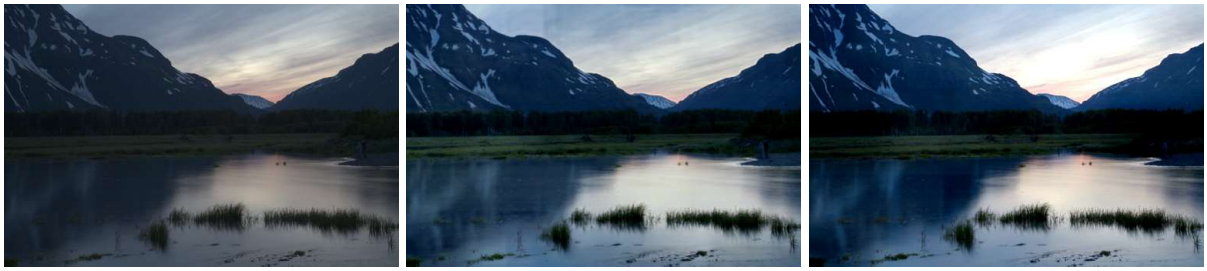

(a) Input (b) U-Net (c) U-Net+Elliptical

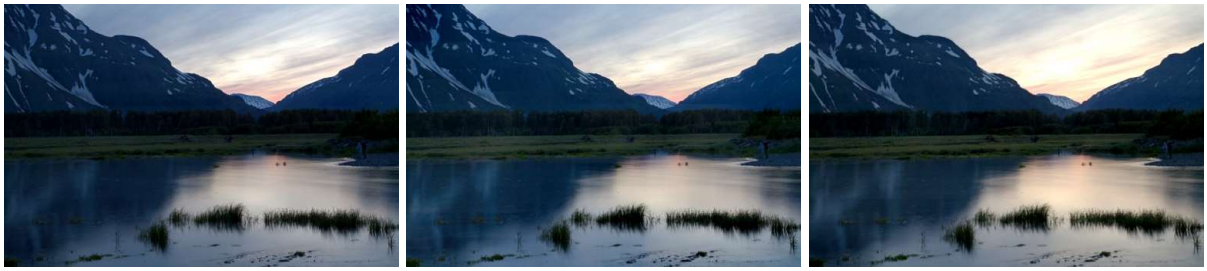

(d) U-Net+Graduated (e) U-Net+Elliptical+Graduated (f) U-Net+Cubic

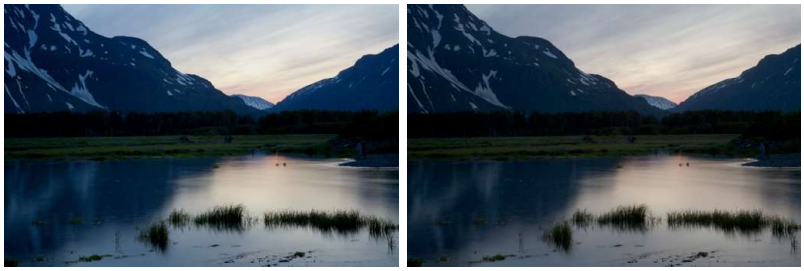

(g) U-Net+Cubic+Elliptical+Graduated (h) Ground Truth

Figure 18: Ablation study showing the effect of different combinations of parametric filter compared to the groundtruth and the baseline U-Net [21] on the **MIT-Adobe5K–DPE** dataset. All cubic filter results are using the 20 parameter per channel cubic filter (cubic-20).

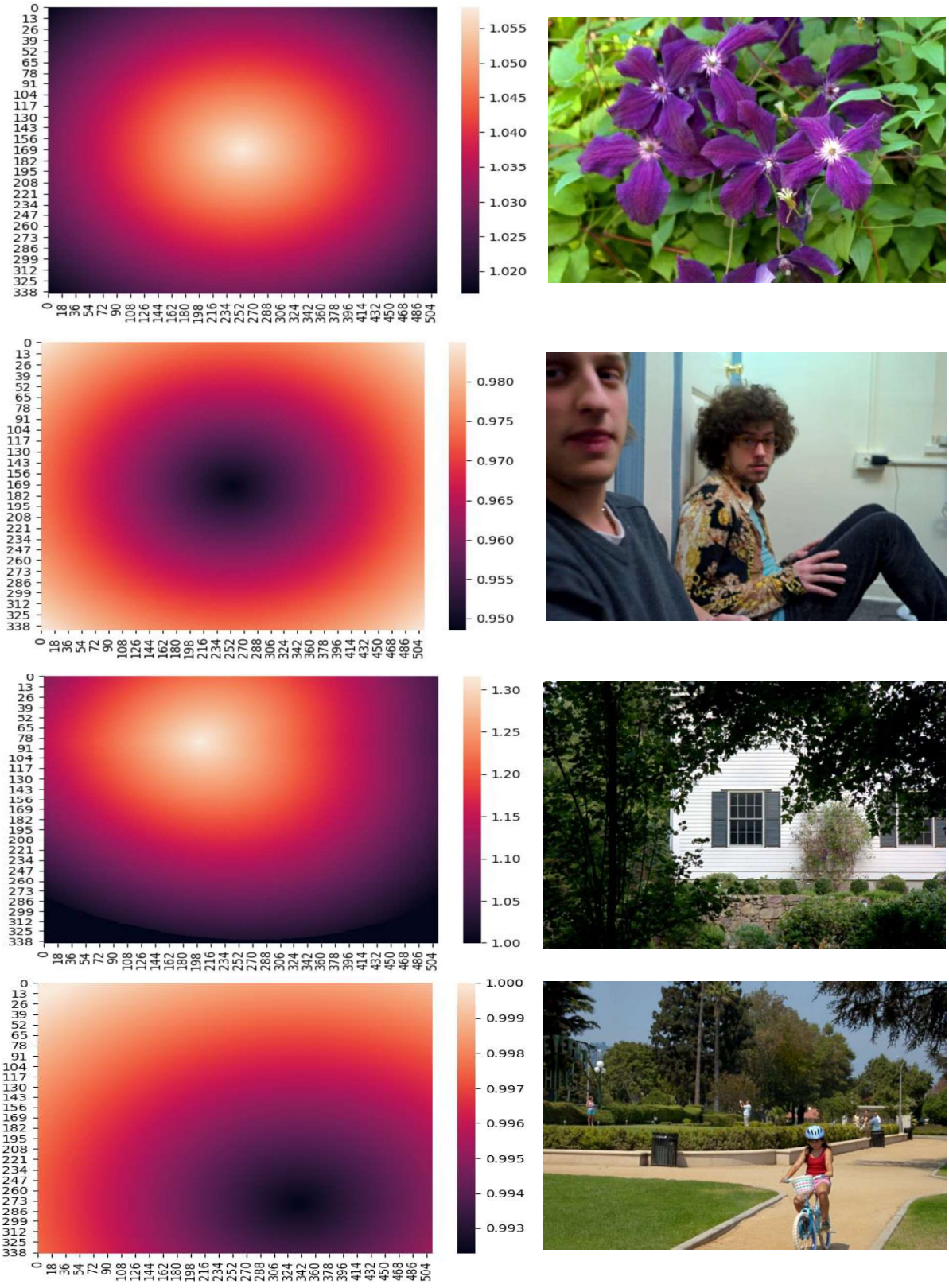

Figure 19: Additional examples of elliptical filters acting on different channels of the input images (from top; 1st row: Green, 2nd row: Blue, 3rd row: Red, 4th row: Red). **Left:** Examples of estimated filters. **Right:** The produced output images. Lighter filter heat map colours correspond to larger image adjustment values. Best viewed in colour.

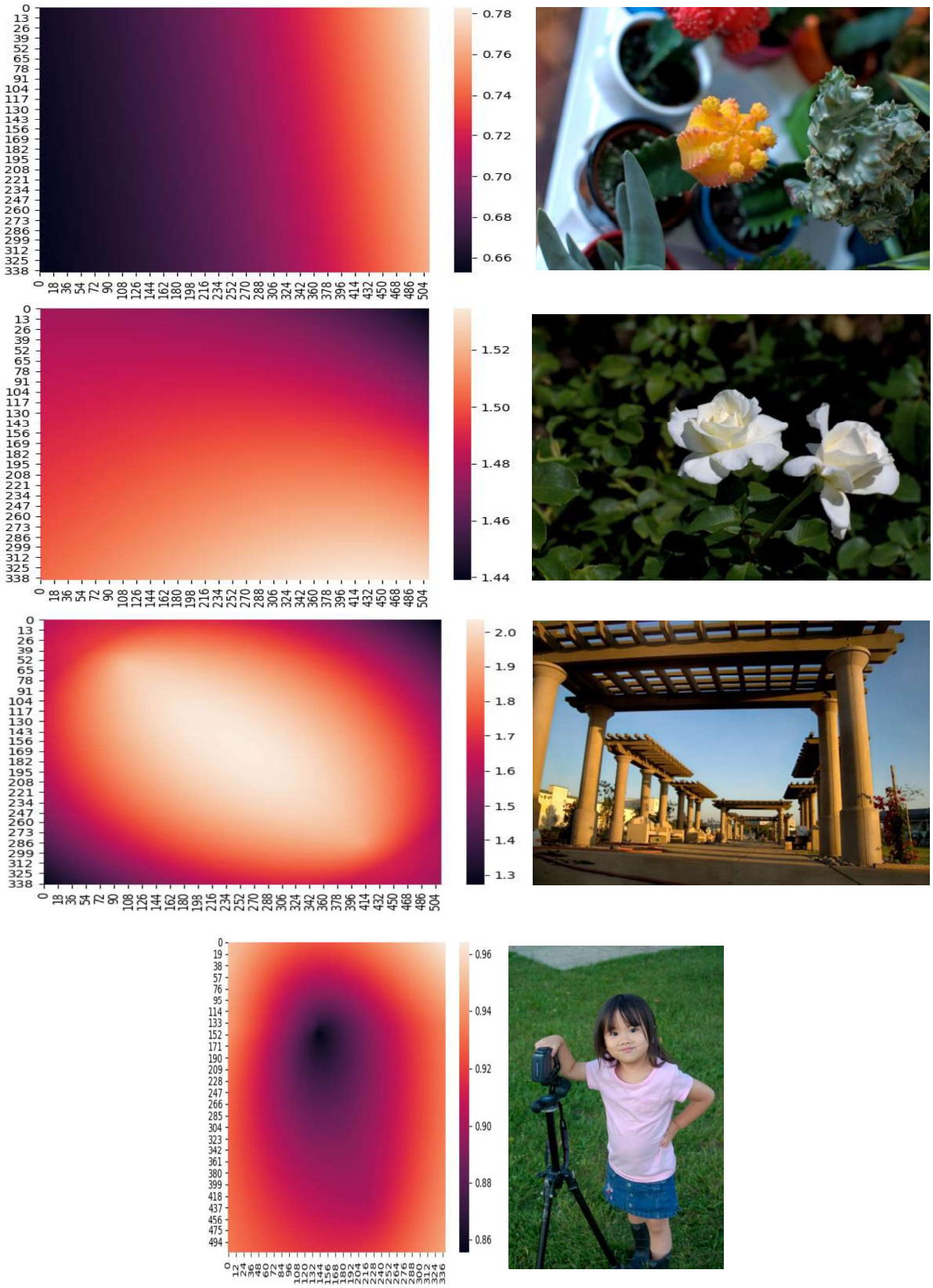

Figure 20: Additional examples of **mixtures of graduated or elliptical filters** acting on different channels of the input images (from top; 1st row: Green, 2nd row: Green, 3rd row: Red, 4th row: Blue). **Left:** Examples of estimated filters. **Right:** The produced output images. Top two rows are mixtures of graduated filters. Bottom two rows are mixtures of elliptical filters. Lighter filter heat map colours correspond to larger image adjustment values. Best viewed in colour.

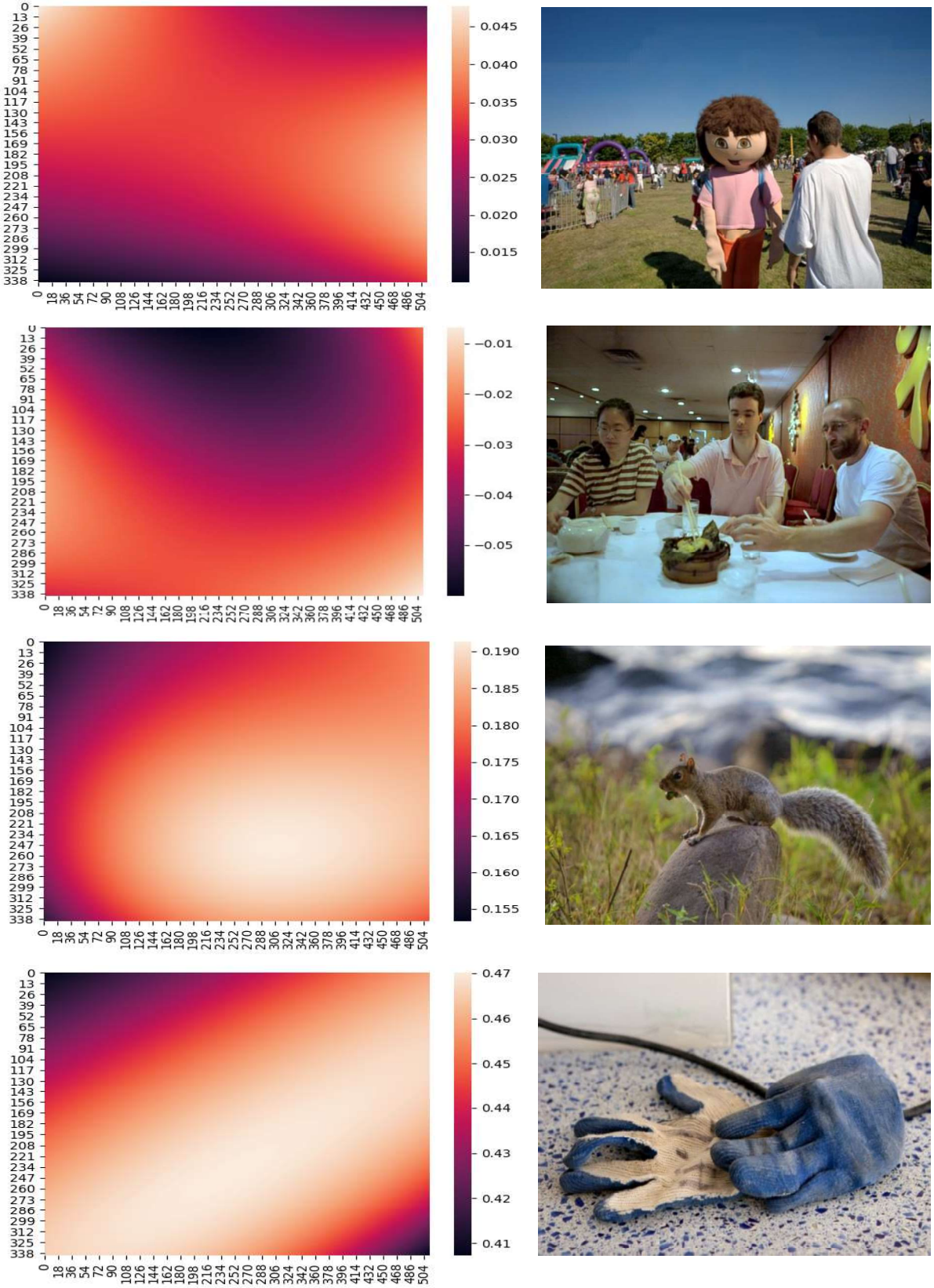

Figure 21: Additional examples of the **cubic-10 filter** acting on different channels (from top; 1st row: Blue, 2nd row: Red, 3rd row: Blue, 4th row: Blue) of the input images. **Left:** Examples of estimated filters. **Right:** The produced output images. Lighter filter heat map colours correspond to larger image adjustment values. Cubic-10 filter is shown without the intensity (i) term. Best viewed in colour.

Figure 22: Example images showing some **DeepLPF failure cases** with respect to the groundtruth. **Top:** It can be observed from the training set distribution that our model has likely learned to brighten human faces. The transformation between the input and groundtruth in this example is uncommon in the MIT-Adobe-5K dataset as artists generally lighten human faces. We note, however, that DeepLPF has removed the reddish colour cast from the input. **Bottom:** Here Artist C increases the saturation of the green hue, however DeepLPF fails to match the same level of saturation. This could be addressed by learning the filters in the Hue-Saturation-Value (HSV) colour space, in which the saturation for a particular hue could be precisely adjusted.